Proceedings of the Combustion Institute 40 (2024) 105746

Contents lists available at ScienceDirect

Proceedings of the Combustion Institute

journal homepage: www.elsevier.com/locate/proci

Analyzing the ignition capabilities of glowing firebrand accumulations

Luqing Zhu, James L. Urban *

Worcester Polytechnic Institute (WPI), 100 Institute Road, Worcester, MA 01609, USA

ARTICLE INFO

Keywords:
Firebrand spotting
Spot ignition
Wildland–urban interface fires
Firebrand accumulation
Glowing combustion

ABSTRACT

Firebrand spotting is a significant mechanism for structure losses in wildland–urban interface (WUI) fires. In this work, the ability of firebrand accumulations to cause flaming ignition of an engineered wood material, Oriented Strand Board (OSB), under different flow conditions was experimentally studied. The firebrands were emulated by burning wooden dowels of two sizes, 6.35 & 12.7 mm. Firebrands were dropped onto on the fuel to form accumulations, with the coverage densities of 0.06 to 0.16 g/cm^2 on the fuel surface. The surface temperature of glowing combustion on the firebrands was measured with color ratio pyrometry. The ignition outcome results show a similar hyperbolic relationship between air flow and coverage density for both firebrand sizes although accumulations of small firebrands can cause the ignition faster. A firebrand combustion model was adopted to predict the surface temperature of accumulated firebrands considering re-radiation between nearby firebrands. A correlation between the ignition time and characteristics of accumulations was also established based on a theoretical combustion and heat transfer analysis.

1. Introduction

Wildland–Urban Interface (WUI) fires, driven by climate change and human expansion into wildland areas, continue to pose a significant threat to communities by causing losses of life and property around the world. One of the primary ways by which wildfires can rapidly spread into WUI communities is via firebrand spotting [1]. Firebrands are typically defined as airborne burning embers (or other hot objects) generated by burning vegetation or other flammable materials in wildfires [2]. They are known to be able to travel long distances by wind and accumulate on combustible structural materials inducing spot fire ignition or igniting fine fuels [3], which increases the difficulty of firefighting and fire protection. Under certain flow and surface conditions, firebrands will accumulate near structures [4,5]. These firebrand accumulations can act as a more competent ignition source than single firebrands [6]. By cooperatively heating the recipient fuel, firebrand accumulations can permit spot ignition to be made possible or faster, compared to a situation with only one (or fewer) firebrand(s) [7,8]. There are an abundance of large-scale experimental studies demonstrating the ability of firebrand accumulations to ignite structural fuels [6,9–12].

Several studies measured the ignition capabilities of firebrand accumulations/groups to ignite materials ranging from fine fuels [13–15] to structural fuels [16–21]. The ignition studies have primarily focused on compact (high coverage density) accumulations, in some cases with firebrands stacked as 2 cm high [17]. These studies found that larger firebrand accumulations [21] and larger coverage densities [17] increased the ignition propensity. The authors previously investigated the critical separation conditions for firebrands to act as a firebrand accumulation through idealized firebrand experiments and physical modeling [16] and similar modeling has also performed by other researchers [22].

Bench-scale studies have considered the heat transfer from single- or accumulated-firebrands to inert substrates or sensors with different measurement methods. It was found that firebrands can cause peak heat fluxes up to 70 kW/m^2 to inert substrates or sensors and the heat flux was found to change depending on the firebrand geometry, pile size, air flow conditions, etc.[19–21,23–26]. Various researchers have used analytical firebrand combustion models for single firebrands, accounting for mass convection limited burning [27], and one study developed and validated an analytical model accounting for the re-radiation effect between firebrands in an array [28]. These studies provide crucial insight into how firebrand accumulations transfer heat to – and ignite – the fuel in this study.

Firebrand accumulation is an important way in which firebrands can ignite structures in wildfires. Research has shown that the ability to cause ignition is strongly dependent on the supply of oxygen by the wind. Similarly, research has shown that firebrand size and proximity of other firebrands can impact of temperature of the firebrands [28], and thus the heat transfer to fuels and their ignition capability [16]. This study seeks to understand how characteristics of the firebrand

* Corresponding author.
E-mail address: jurban@wpi.edu (J.L. Urban).

https://doi.org/10.1016/j.proci.2024.105746
Received 4 December 2023; Accepted 15 July 2024
Available online 21 August 2024

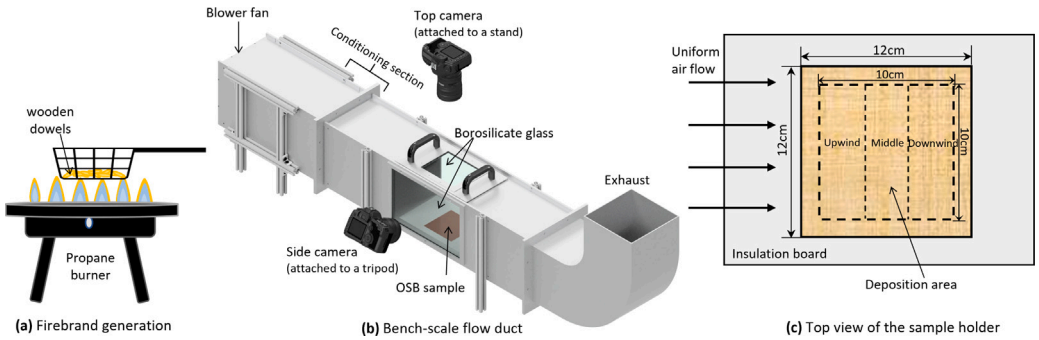

Fig. 1. (a) Firebrand generation setup, (b) Bench-scale flow duct with associated instrumentation and removable lid for depositing firebrands, (c) schematic up of the fuel surface. (figures not to scale).

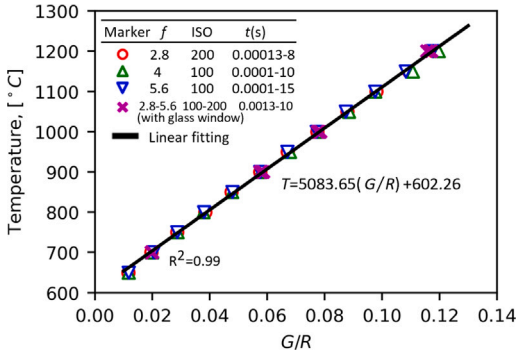

Fig. 2. Ratio pyrometry calibration curve.

accumulation (size of firebrands, accumulation coverage density) and wind impact the oxygen-limited heat release of the firebrands and heating and ignition of the fuel. This is investigated through experiments with a structural fuel, Oriented Strand Board (OSB), two firebrand sizes, four coverage densities, and six air flow speeds. Ratio pyrometry is used to monitor the combustion of the firebrands, and analytical models are used to characterize the combustion behavior of the firebrand and the ignition of the fuel. From these models a physical correlation is developed explaining the ignition time results.

2. Experiment description

2.1. Experimental setup and procedures

The experimental setup is shown in Fig. 1, which consists of a firebrand preparation setup and a bench-scale flow duct for ignition tests. The duct has a 20×20 cm^2 cross section with a variable-speed blower fan that can generate air flows in the range of 0.5–3.0 m/s. The air speeds are intended to be similar in magnitude to calculated local air flow speeds near accumulations and estimates of critical windspeeds for firebrands to be pushed along the floor, 2.3 m/s [4,5]. A honeycomb insert and several mesh screens in the conditioning section are used to ensure uniform flow into the test section. The flow within the test section was verified using a hot wire anemometer before the tests in the absence of firebrands. Borosilicate glass windows on both sides and above the sample allow visual access to sample and firebrands.

As seen in Fig. 1c, the fuel is 12×12 cm^2 and mounted flush along the centerline of the floor. Firebrands were deposited on the central 10 × 10 cm^2 testing area on the sample surface. The fuel, Oriented Strand Board (OSB) with a thickness of 11 mm, was found to have a density of 609 ± 28 kg/m^3. The fuel was oven dried (100 °C for 12 h) before tests to remove moisture (FMC ≈ 0%) with no detectable change in mass with further oven drying. A side-view camera was employed to capture ignition events of the fuel. The surface temperature of glowing portions of the firebrand accumulation were measured with color ratio pyrometry using a top-view camera (Sony RX10 M4).

Cylindrical yellow pine wooden dowels of two diameters, d=12.7 & 6.35 mm, both 25 mm long were used to emulate smoldering firebrands in wildfires. Before preparation, the virgin dowels had an oven-dry density of 590 ± 45 kg/m^3. At the start of tests, the firebrands were prepared by exposing a desired initial mass of dowel pieces in a wire mesh basket to a propane flame [19,21]. The burner was turned off after approximately 120 s, allowing flaming dowels to burn freely and transition into glowing firebrands (no visible flames). In this work, glowing combustion was considered to be a form of smoldering combustion where high surface temperatures in excess of approximately 600 °C causing the fuel surface to incandesce. In the present scenario this is enabled by the absence of endothermic pyrolysis reactions and the presence of forced convection of oxygen to the fuel surface.

A thin insulation board held vertically above the funnel center was used to remove the horizontal momentum of firebrands ensuring a relatively uniform deposition without firebrands piling on only one part of the fuel in every test. This approach was found to produce repeatable deposition without preferential landing of firebrands. Note that the exact arrangement of deposited firebrands was still random. The initial deposited mass of different firebrand coverage densities was estimated by quenching glowing firebrands in a water pan. The firebrand samples collected from different initial masses were measured to have no significant difference in average size and mass. The size (projected area and mass) of the firebrands overlaps with measurements of firebrands generated by structural fuels [8] and vegetation [29]. For each firebrand size, four different coverage densities, ϕ, ranging from 0.05 to 0.16 g/cm^2 were studied (roughly 16–292 firebrands were deposited depending on the cases), representing conditions from loose accumulation that does not cover the entire test area to conditions where firebrands noticeably stack one another (i.e., firebrand pile). Each case was repeated 6 to 14 times with a total of over 300 tests performed.

2.2. Color ratio pyrometry

Color ratio pyrometry has been used as an optical method to measure the surface temperature of glowing particles/firebrands with an advantage that it does not require the knowledge of firebrand and ash layer's surface properties [27,30,31]. It can be accomplished with a digital color camera with a built-in bayer filter array that separates light into red, green and blue color channels which are the combined intensity of incoming light in three different overlapping spectral bands corresponding to each color channel. The temperature measurement is achieved by measuring a ratio of two color channel intensities and determining the black body temperature that produces same observed intensity ratios. Relating the temperature of the glowing firebrand to the color ratio can be achieved through a thorough characterization

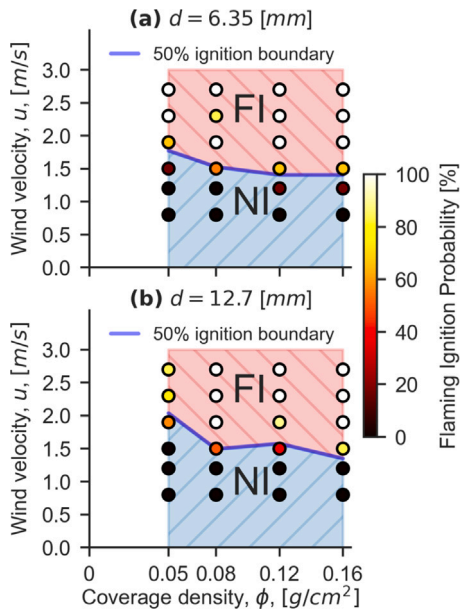

Fig. 3. NI and FI regimes of OSB exposed to firebrands of two sizes (a) d=6.35 mm & (b) d=12.7 mm. Circles are colored according to the observed FI probability with a colorbar and 50% FI probability is shown with blue line. (For interpretation of the references to color in this figure legend, the reader is referred to the web version of this article.)

of the camera spectral response [27] or calibration with a blackbody radiation source [30,32]. In this study the calibration with a blackbody radiation source is used.

The surface temperature of firebrands is determined by finding the temperature that produces the same predicted color ratio based on the calibration curve. For hot objects such as glowing firebrands, the ratio G/R was selected for curve fitting because it yields the highest signal-to-noise ratios. As seen in Fig. 2, the temperature is correlated as a linear function of G/R (black line in Fig. 2) and the borosilicate glass window was found to have a no significant effect on the correlation. The details of applying pyrometry techniques for firebrands can be seen in Refs. [27,30].

3. Results

3.1. Ignition results

Each test resulted in one of two possible outcomes: No Ignition (NI) or sustained Flaming Ignition (FI). Smoldering Ignition (SI) was not studied as there is no clear evidence of self-sustaining smoldering of the OSB fuel leading up to ignition in the experiments. The observed FI probability, $\hat{p}_{FI}$, is the fraction of replicate tests resulting in FI. In this study, FI was determined by visual observation of persistent flames attached on the exposed fuel surface. Furthermore, preliminary experiments were conducted on an inert substrate and smoldering-to-flaming transition of firebrands was not observed from the deposited firebrands within the range of air flow speeds in this study. Thus, smoldering to flaming transition of the firebrand was not analyzed here. Fig. 3 shows the ignition results as an observed FI probability noted by the color. Logistic regression was used to find the FI/NI boundary where the FI probability, p_{FI}=50%. The logistic function, $p_{FI}=1/(1+e^{-f})$, with $f=a+bU$ for each firebrand size, d, and coverage density, ϕ, is used to obtain the critical air speeds. The FI/NI boundary lies where f=0 and is found by connecting these points with straight lines. It is seen from Fig. 3 that the FI/NI boundaries exhibit a shallow hyperbolic relationship between the coverage density and flow speed although the boundary for large firebrand size is less consistent.

In general, the ignition results including time to ignition, showed greater variation for the larger firebrand size. The FI/NI boundary in Fig. 3b shows non-monotonic behavior with varying coverage density, which is attributed to the fact that the *number* of firebrands deposited is less than for the smaller size at the same ϕ and hence entails more random firebrands deposition on the fuel. Within the range of coverage densities examined in this work, the FI/NI boundaries for both sizes are seen to be similar, with the required air speed roughly in the range of 1.5–2.0 m/s. When the air speed is at or below 1.2 m/s, FI is not observed or occurs with low probability ($\hat{p}$<20%). For the smaller firebrand size, it is also seen that the boundary is flatter, demonstrating that the ignition capability of firebrand accumulations is significantly less sensitive to coverage density compared to wind. This behavior is less clear for large firebrand size in the current study, but it appears to follow the same trend.

The impact of air flow on the observed ignition capability is similar to other studies examining the ability of firebrand groups to ignite OSB, but there are differences. The present work finds a similar critical wind speed for FI as one study [18], however that study found increasing the wind speed yields non-monotonic behavior in ignition probability with u=2.7 m/s yielding an 11% ignition probability while the most similar conditions in this study find 100% FI probability. This previous study employed a sample width of 50 mm, half that of the current study and reported that the length of the sample facing the incoming air flow had a large effect on the observed ignition probability. The larger sample width was found to provide more local sites for local ignitions to occur and thus more chances for a given test to result in FI [18]. Another study [19] observed a monotonic trend of FI probability with air speed, as seen in the present study, but saw infrequent FI events at lower flows.

The mean times to FI of the OSB from replicate tests are summarized in Fig. 4a & b. The dependence of time to FI on the flow speed, u, and the firebrand coverage density, ϕ, is clearly seen from the trend, with higher coverage density and air speed resulting in shorter time to ignition. All observed FIs induced by accumulations of small firebrands took place during the first 20 s of the test, while large firebrand tests with the same ϕ took longer. There are several possible effects to explain this finding. First, the surface area to volume ratio of the smaller firebrands is roughly twice as large for the larger firebrand size. Thus, because the combustion of the firebrands is assumed to be limited by convective transport of oxygen, the heat release per unit mass of firebrands (or for a given ϕ) will be higher (approximately twice) for the smaller size. Similarly, the projected area of the firebrand accumulation to mass ratio of firebrands is also approximately twice that for the large firebrand size. This effect essentially means that the smaller firebrands accumulate over a greater portion of the fuel surface compared to larger firebrands at the same ϕ and as a result the gaps between firebrands are small, which was observed in the experiments. With the increased proximity of the firebrands, there should be a stronger cooperative ignition effect [16] and the radiative heat losses of the firebrands should be smaller because the firebrand will re-radiate to each other [28].

Fig. 4c & d shows typical FI cases and all of the ignitions were observed to occur in the upwind area nearest the incoming air flow and undergo the strongest glowing combustion. In the experiments, the majority of the flames were seen to emerge from underneath or between neighboring firebrands and multiple ignitions were observed in the upwind area at large flow speed. Fig. 4e & f shows the flame duration for cases resulting in an FI outcome. It is clearly seen that the flame duration increases with airflow and generally with coverage density. It is noticeable that the flames sustain significantly longer on the fuel surface for the large firebrand cases although the ignition process by accumulations of small firebrands is shorter. This is believed to be because the burnout time of glowing firebrands should increase with size [28].

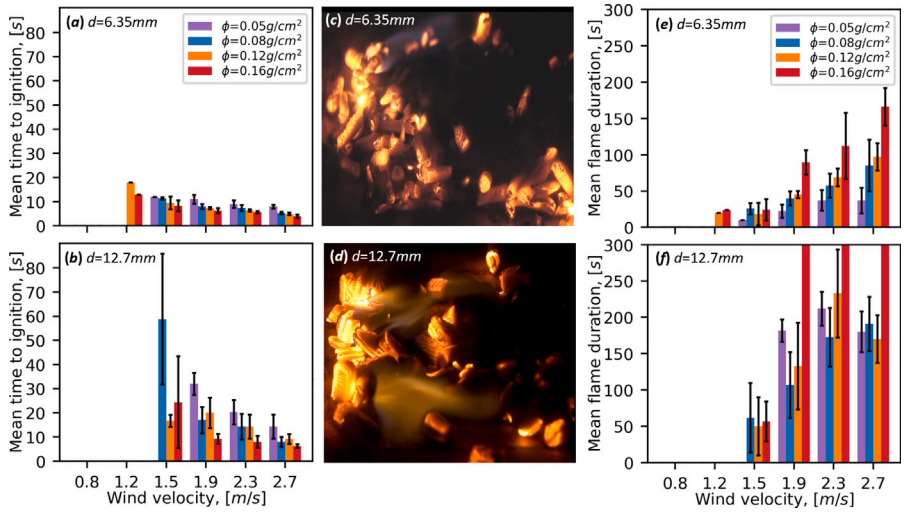

Fig. 4. (a) & (b) show the mean times to FI of the OSB for both firebrand sizes. Error bars indicate ±1 standard deviation from replicate tests. (c) & (d) display typical FI cases ($\phi = 0.12$ g/cm^2; $u = 2.3$ m/s) in the experiments. FI was observed to occur within the upwind area of fuel. (e) & (f) show mean flame duration on the fuel surface after FI occurs. Flames were manually extinguished as they lasted over 300 s. (For interpretation of the references to color in this figure legend, the reader is referred to the web version of this article.)

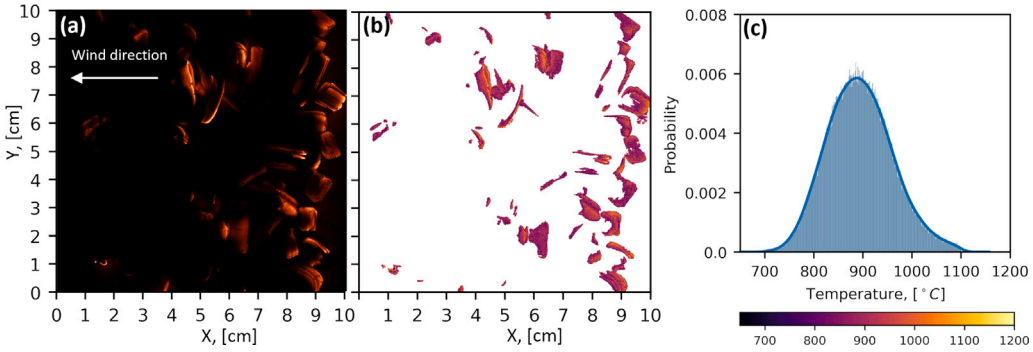

Fig. 5. Color ratio pyrometry results from a representative case (d = 12.7 mm; ϕ = 0.12 g/cm^2; u = 2.3 m/s). The cropped area shown is the deposition area of the fuel bed (10×10 cm^2). (a) shows a color snapshot (*JPEG*) taken immediately after the flow duct was sealed. (b) & (c) plot the corresponding surface temperature and distribution of glowing combustion temperatures. The mean glowing temperature in this case is obtained as 897 ± 67 °C. (For interpretation of the references to color in this figure legend, the reader is referred to the web version of this article.)

3.2. Glowing combustion of firebrands

The surface temperatures of glowing combustion in firebrand accumulations under different flow speeds were measured using color ratio pyrometry as shown in Fig. 5. Images of glowing firebrands deposited on the fuel surface were taken at an interval of 10s after the flow duct was closed after deposition. For applying color pyrometry, the ratio G/R was found for each pixel in the images and then the temperatures were calculate according to calibration function (Fig. 2). Pixel temperatures outside the range 650–1200 °C were removed. A challenge in this work is that portions of the fuel surface were illuminated by firebrands undergoing strong glowing combustion and could report false temperature within an accumulation of low coverage density. A threshold value of the green channel was found to remove most of the reflections because the reflected light is much dimmer than that from glowing firebrands. In addition, an imaging processing algorithm (skimage.morphology.remove_small_objects) was applied to remove reflection, leaving a small fraction of reflection pixels (on average < 2% of the total glowing pixels). These remaining pixels of reflected light are expected to have a small impact on the average temperature because the spectrum of the light should be similar to that from the glowing combustion.

Fig. 5 presents an example of temperature measurement results for a firebrand accumulation. Fig. 5b shows the temperature of glowing firebrand surfaces by color ratio pyrometry and the glowing combustion activity of imaged firebrands (Fig. 5a). It can be seen that most of the glowing combustion appear in the upwind area with less glowing surfaces observed in the middle and downstream area. This is attributed to the decrease in oxygen supply to the firebrand surfaces along the flow direction as the oxygen is consumed by glowing combustion. Because the glowing combustion is rate limited by oxygen, the heat release correspondingly decreases along the flow direction. The glowing temperatures range between 700–1100 °C as is seen from the temperature distribution of pixels in Fig. 5c, which is similar to previous research [27,28,30] of suspended firebrands. It however should be noted that this temperature does not represent the average temperature of the *entire accumulation* because there are portions of firebrands within the accumulation that are not hot enough to visibly incandesce.

Fig. 6 shows the mean glowing surface temperature of firebrands in the upwind area during the first 80 s for different coverage densities and flow speeds. The upwind area is where the ignition of fuel occurs and thus is of significant interest in this study. A trend of glowing temperature increasing with flow speed is seen for both firebrand sizes, with the mean glowing temperature up to 930 °C at 2.7 m/s. For

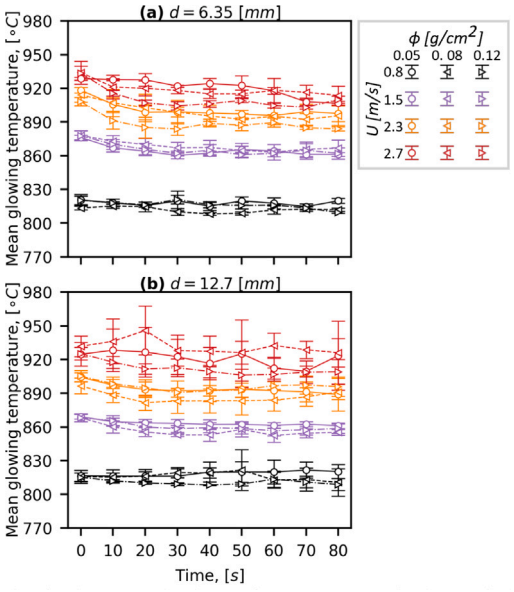

Fig. 6. The mean glowing surface temperature in the upwind area over the first 80 s for both firebrand sizes. Error bars show ±1 standard deviation from replicate tests.

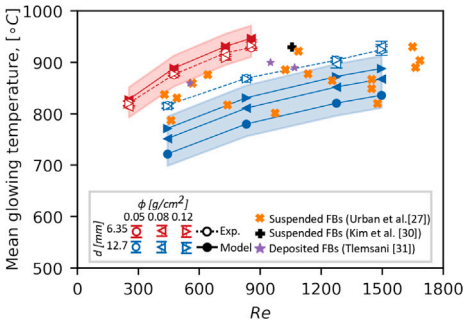

Fig. 7. Comparison of temperatures from model and experiments. Shaded regions marking the variance of temperature predictions if the emissivity is changed by ±0.1. References include temperature measurement by ratio pyrometry on firebrands with similar diameters in this study.

each firebrand size, different coverage densities under same air flow conditions have similar temperatures.

4. Discussion

4.1. Accumulated firebrand combustion model

To better understand the experimental results, a convection driven firebrand combustion model is adopted from the literature [28] to calculate the surface temperature of glowing firebrands within an accumulation under forced convection. The reader is referred to Ref. [28] for more detail and discussion of the model. However, the surface energy balance of a deposited firebrand in an accumulation is modified as:

$$\dot{q}''_{\mathrm{HRR}} A_s = \dot{q}_{FB\to\infty} + \dot{q}_{FB\leftrightarrow FB} + \dot{q}_{FB\to fu} \tag{1}$$

where $\dot{q}''_{\mathrm{HRR}}$ is the heat release rate of the char oxidation reaction, calculated as $\dot{m}''_c \Delta h_c$, A_s is the firebrand surface area, $\dot{q}_{FB\to\infty}$ is the radiation and convection heat loss from the firebrand to the ambient; the heat transfer to the fuel, $\dot{q}_{FB\to fu}$, is assumed to be primarily through radiation because of the very small contact area between the firebrand and fuel surface [33,34]. The firebrands are assumed to be distributed with even space between them and exchange no net heat as two neighboring hot firebrands of close proximity re-radiate mutually, $\dot{q}_{FB\leftrightarrow FB}\approx 0$. Thus Eq. (1) becomes:

$$\dot{m}''_c \Delta h_c = h(T_{FB} - T_\infty) + \varepsilon\tau\sigma(1-2F)(T_{FB}^4 - T_\infty^4) \tag{2}$$

where Δh_c is the heat of combustion for wood char; h is the convective heat transfer coefficient, T_{FB} and T_∞ are glowing and ambient temperatures; $\varepsilon\tau$ is the product of the char emissivity and ash transmissivity, 0.7 [27,30]; σ is the Stefan–Boltzmann constant; F is the view factor between two firebrands, estimated using two separated parallel cylinders. F depends on the coverage density varying from 0.07–0.18 and 0.16–0.18 for large and small firebrands sizes respectively. The convective burning rate of the char surface is given as [28]

$$\dot{m}''_c = \rho_\infty Nu D_{\mathrm{O_2/air}} \ln(1+B)/d_0 \tag{3}$$

where ρ_∞ is the ambient air density; $D_{\mathrm{O_2/air}}$ is the diffusion coefficient of oxygen in air; B is the Spalding mass transfer number, approximated as $B = Y_{o_2,\infty}/r_0$; r_0 is the oxygen-to-fuel ratio, taken as 2 [28]; d_0 is the initial firebrand diameter. The heat transfer coefficient is estimated with the Nusselt number, $h = \mathrm{Nu}\cdot k/d_0$, where Nu was found using the correlation [33], $\mathrm{Nu} = 0.683\mathrm{Re}^{0.466}\mathrm{Pr}^{1/3}$, where Pr is the Prandtl number of air, $\mathrm{Re} \equiv ud_0/\nu$ is the Reynolds number, u is the flow speed; ν is the kinematic viscosity of ambient air. The surface temperature of glowing firebrands is obtained by solving Eq. (2) for each test condition.

Fig. 7 compares the temperature from the model to the measurement by ratio pyrometry. It is seen that the model results overall agree qualitatively with the experimental measurement, with surface temperature increasing with Re and higher temperatures observed for the smaller firebrands. Good quantitative agreement is observed for the small firebrand size, but the agreement for the large firebrand size is less good. In the pyrometry measurements, a significant trend with coverage density was not observed, in contrast the model predicts large effect of coverage density for the larger firebrand size from re-radiation effects which is not observed in the measurements.

As mentioned earlier, the large firebrand tests consistently showed less repeatable results compared to the smaller firebrand tests. One explanation is that the projected area of larger firebrands was roughly half that of the small firebrands. Thus, more of the fuel surface was not covered by the accumulation and thus the gap between large firebrands could vary more. In addition, for the complex scenario studied in this work, there are other aspects that could influence the glowing combustion of the firebrands of all sizes including the random deposition of firebrands, change of morphology (firebrands may shatter), and complicated airflow over firebrands. These aspects could possibly change the magnitude of convective mass transport of oxygen to the glowing firebrand surfaces surface and subsequently impact the local surface temperature of firebrands within an accumulation, which is not accounted for in the Nusselt number correlation employed in this work. A more detailed treatment of the convective mass transfer to a group of randomly deposited firebrands could allow for better prediction of the glowing behavior in the downwind areas of the accumulation. However the random accumulation geometry makes it difficult to resolve this process in detail. Recent research has moved towards this direction, finding Nusselt number correlations for well-arranged individual – and groups – of cylinders laying on the floor of a flow duct [35]. In this work they find that the mass transfer (i.e., Nusselt number to firebrands toward the leading-edge and top of the pile are higher than the downstream firebrands like is observed in the experiments (e.g., Fig. 5).

4.2. Ignition phenomena

A theoretical analysis was developed to investigate the dependence of ignition capability of firebrand accumulations on the firebrand size, d, the coverage density, ϕ, and air flow, u. The heat transfer process

after the firebrands are deposited on the fuel can be expressed as the energy balance of the heated portion of the fuel surface starting from state right after deposition to the moment of ignition. Based on the observation that FI occurs in the upwind area of the fuel bed, an assumption is made such that glowing firebrands within the upwind area play a primary role in heating of the fuel. It is assumed that the glowing combustion acts as an ignition pilot, and thus flaming ignition occurs when the fuel temperature reaches the pyrolysis temperature, T_p.

$$(c\rho)_f A_{up}\delta(t)(T_p-T_\infty)=Q_{FB\to fu}-Q_{fu\to\infty} \tag{4}$$

where $\delta(t)=\sqrt{t_{ign}k_f/(\rho c)_f}$ is the portion of the fuel heated before ignition or the thermal penetration depth, k_f, c_f and ρ_f are the fuel thermal conductivity, heat capacity and density respectively; A_{up} is the upwind fuel area (Fig. 1c); $Q_{fu\to\infty}$ is the convection and radiation heat transferred from the fuel to the ambient; $Q_{FB\to fu}$ is primarily radiation heat transferred from firebrands to the fuel. From 0s $\to t_{ign}$, $Q_{FB\to fu}$ is therefore described as:

$$Q_{FB\to fu}\propto Q_{\mathrm{HRR,acc}}=nA_s\dot{q}''_{\mathrm{HRR}}t_{ign} \tag{5}$$

where n is the number of the glowing firebrands in the upwind area; A_s is the firebrand surface area; $\dot{q}''_{\mathrm{HRR}}$ is obtained from Eq. (1).

It is assumed that before ignition, $Q_{fu\to\infty}$ is small in part because a significant portion of the fuel surface is covered by firebrands which also obstruct airflow from cooling the entire surface. Substituting Eq. (5) into Eq. (4) yields:

$$\frac{1}{\sqrt{t_{ign}}}\propto\frac{nA_s\dot{q}''_{\mathrm{HRR}}}{A_{up}\sqrt{(k\rho c)_f}(T_p-T_\infty)} \tag{6}$$

which can be rewritten using the coverage (projected) area of a firebrand on the fuel surface, $A_c\approx d_0L_0$.

$$\frac{1}{\sqrt{t_{ign}}}\propto\frac{\psi\pi\dot{q}''_{\mathrm{HRR}}}{\sqrt{(k\rho c)_f}(T_p-T_\infty)} \tag{7}$$

with ψ defined as the accumulation factor which describes the firebrands coverage conditions from accumulation of different coverage densities. It is calculated assuming uniform firebrand landing as:

$$\psi=\frac{nA_c}{A_{up}}=\frac{4\phi}{\pi d_0\rho_{FB}} \tag{8}$$

where ρ_{FB} is the average glowing firebrand density from the experiments. Inspection of ψ reveals that the firebrands within an accumulation would occupy the entire test area and noticeably stack up as a pile when $\psi > 1$, otherwise it could be considered as a loose accumulation. This is overall consistent with the appearance features of different accumulations observed from the experiments, with ψ varying from 0.3–1.2 for large firebrand size and 0.7–2.1 for small firebrand size. Substituting Eq. (8) into Eq. (7):

$$\frac{1}{\sqrt{t_{ign}}}\propto\frac{4\phi\rho_\infty NuD_{\mathrm{O_2/air}}\ln(1+B)}{d_0^2\rho_{FB}\sqrt{(k\rho c)_f}(T_p-T_\infty)} \tag{9}$$

Fig. 8 shows a linear relationship between $1/\sqrt{t_{ign}}$ and the right hand term of Eq. (9) which includes the effect of ϕ, d_0&u. The correlation based on the steady-state analysis captures the time to ignition by accumulations of both firebrand sizes qualitatively, but there is still scatter. This could be attributed to less consistent ignition results (i.e., large uncertainty of ignition time at low FI probability) or more complex firebrand combustion dynamics not considered in this analysis. It also should be noted that the time-dependent nature of firebrand exposure is not considered in this analysis but has been investigated empirically and numerically [18,36,37]. Including the transient aspect of heat exposure from firebrand accumulations could be important for quantitatively predicting the susceptibility of combustible recipient fuels.

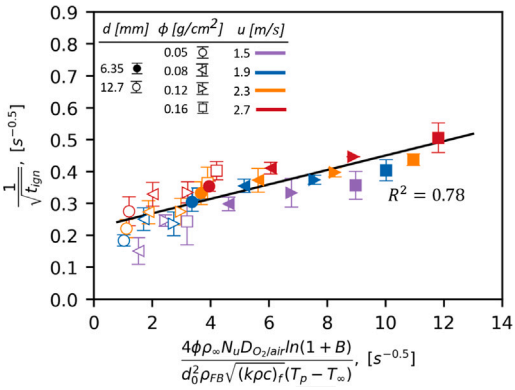

Fig. 8. Correlation between $1/\sqrt{t_{ign}}$ and $f(\phi, d_0, \dot{q}''_{FB})$.

5. Conclusion

Experiments investigating the glowing combustion activity of firebrand accumulations and their ignition capabilities have been conducted over two firebrand sizes, four accumulation coverage densities and six air flow speeds. The accumulations studied here are representative of different coverage situations ranging from loose accumulations to compact piles. Surface temperatures of glowing firebrands were measured by ratio pyrometry. The results reveal that air flow is the dominant factor of glowing temperatures of accumulated firebrands and a convection-driven combustion model was adopted to study the dependence of air flow and re-radiation effects on the temperature of deposited firebrands within accumulations.

Critical conditions are identified under which accumulations with different coverage densities and firebrand sizes would ignite a structural fuel (OSB) under air flow. The ignition results show similar FI/NI boundaries for both firebrand sizes. However, at the same coverage density and air flow, the time to ignition from accumulations of the larger firebrands are longer. Through analytical modeling of the firebrand and fuel, it is found that the time to ignition is controlled by the firebrand combustion behavior and subsequent heat transfer to the fuel, both of which are strongly impacted by the size and air speed as well as coverage density to a lesser degree.

Novelty and significance statement

This research presents a novel data-set of well characterized firebrand accumulation experiments which are analyzed using analytical physical models of the accumulated firebrands burning and the fuel ignition processes. We believe the models capture the important physical mechanisms for the fuel ignition process. This is significant because prior bench-scale studies have only reported direct measurements, developed purely empirical relationships, or measured heat transfer from firebrands to inert substrates or sensors. Moreover, the present study considers a broader parameter space (wind, firebrand size, and accumulation density) with finer parameter resolution along with novel accumulation measurements and analysis of firebrand accumulations.

CRediT authorship contribution statement

Luqing Zhu: Performed the experiments, Developed experimental procedure, Analyzed data, Completed modeling, Wrote first draft. **James L. Urban:** Designed and led the research, Edited the manuscript.

Declaration of competing interest

The authors declare that they have no known competing financial interests or personal relationships that could have appeared to influence the work reported in this paper.

Acknowledgments

This work was funded by WPI, USA and the National Science Foundation (NSF), USA award #2138619.

References

[1] S.E. Caton, R.S. Hakes, D.J. Gorham, A. Zhou, M.J. Gollner, Review of pathways for building fire spread in the wildland urban interface part I: Exposure conditions, Fire Technol. 53 (2017).
[2] V. Babrauskas, Firebrands and embers, Encyclopedia Wildfires Wildland-Urban Interface (WUI) Fires (2018) 1–14.
[3] A.C. Fernandez-Pello, C. Lautenberger, D. Rich, C. Zak, J. Urban, R. Hadden, S. Scott, S. Fereres, Spot fire ignition of natural fuel beds by hot metal particles, embers, and sparks, Combust. Sci. Technol. 187:1-2 (2015) 269–295.
[4] S. Suzuki, S.L. Manzello, Experimental investigation of firebrand accumulation zones in front of obstacles, Fire Saf. J. 94 (April) (2017) 1–7.
[5] S. Suzuki, S.L. Manzello, Investigating the effect of structure to structure separation distance on firebrand accumulation, Front. Mech. Eng. 6 (2021).
[6] S. Suzuki, S.L. Manzello, Role of accumulation for ignition of fuel beds by firebrands, Appl. Energy Combust. Sci. 1–4 (June) (2020) 100002.
[7] E. Koo, P.J. Pagni, D.R. Weise, J.P. Woycheese, Firebrands and spotting ignition in large-scale fires, Int. J. Wildl. Fire 19 (7) (2010) 818–843.
[8] S. Suzuki, S.L. Manzello, Characteristics of firebrands collected from actual urban fires, Fire Technol. 54 (2018) 1533–1546.
[9] S.L. Manzello, S. Suzuki, Experimental investigation of wood decking assemblies exposed to firebrand showers, Fire Saf. J. 92 (2017) 122–131.
[10] S.L. Manzello, S. Suzuki, Y. Hayashi, Enabling the study of structure vulnerabilities to ignition from wind driven firebrand showers: A summary of experimental results, Fire Saf. J. 54 (2012) 181–196.
[11] S.L. Manzello, S.-H. Park, S. Suzuki, J.R. Shields, Y. Hayashi, Experimental investigation of structure vulnerabilities to firebrand showers, Fire Saf. J. 46 (8) (2011) 568–578.
[12] S. Suzuki, S.L. Manzello, On unraveling community ignition processes: Joint influences of firebrand showers and radiant heat applied to fuel beds, Combust. Sci. Technol. 195 (13) (2023) 2989–3002.
[13] S.S. Wessies, M.K. Chang, K.C. Marr, O.A. Ezekoye, Experimental and analytical characterization of firebrand ignition of home insulation materials, Fire Technol. 55 (3) (2019) 1027–1056.
[14] D.P. Kasymov, A.I. Filkov, D.A. Baydarov, O.V. Sharypov, Interaction of smoldering branches and pine bark firebrands with fuel bed at different ambient conditions, in: SPIE, Tomsk, Russia, 2018.
[15] S.L. Manzello, S.H. Park, T.G. Cleary, Investigation on the ability of glowing firebrands deposited within crevices to ignite common building materials, Fire Saf. J. 44 (6) (2009) 894–900.
[16] L. Zhu, J.L. Urban, Cooperative spot ignition by idealized firebrands: Impact of thermal interaction in the fuel, Fire Saf. J 135 (2023) 103701.
[17] J.A. De Beer, J.A. Alascio, S.I. Stoliarov, M.J. Gollner, Analysis of the thermal exposure and ignition propensity of a lignocellulosic building material subjected to a controlled deposition of glowing firebrands, Fire Saf. J 135 (2023) 103720.
[18] J.A. De Beer, E.L. Dietz, S.I. Stoliarov, M.J. Gollner, An empirical firebrand pile heat flux model, Fire Saf. J 141 (2023) 104004.
[19] H. Salehizadeh, R.S.P. Hakes, M.J. Gollner, Critical ignition conditions of wood by cylindrical firebrands, Front. Mech. Eng. 7 (March) (2021) 1–13.
[20] F. Richter, B. Bathras, J. Barbetta Duarte, M.J. Gollner, The propensity of wooden crevices to smoldering ignition by firebrands, Fire Technol. (2022).
[21] R.S. Hakes, H. Salehizadeh, M.J. Weston-Dawkes, M.J. Gollner, Thermal characterization of firebrand piles, Fire Saf. J. 104 (2019) 34–42.
[22] O. Matvienko, D. Kasymov, E. Loboda, A. Lutsenko, O. Daneyko, Simulation of the impact of firebrands on the process of the wood layer ignition, Fire 6 (4) (2023) 148.
[23] Z. Tao, B. Bathras, B. Kwon, B. Biallas, M.J. Gollner, R. Yang, Effect of firebrand size and geometry on heating from a smoldering pile under wind, Fire Saf. J. 120 (April) (2020) 103031.
[24] E.D. Bearinger, J.L. Hodges, F. Yang, C.M. Rippe, B.Y. Lattimer, Localized heat transfer from firebrands to surfaces, Fire Saf. J. 120 (April) (2020) 103037.
[25] Y.M. Abul-Huda, N. Bouvet, Thermal dynamics of deposited firebrands using phosphor thermometry, Proc. Combust. Inst. 38 (3) (2021) 4757–4765.
[26] A.E. Mensch, S.S. Wessies, A. Hamins, J.C. Yang, Measuring firebrand heat flux with a thin-skin calorimeter, Fire Saf. J. 140 (June) (2023) 103859.
[27] J.L. Urban, M. Vicariotto, D. Dunn-Rankin, A.C. Fernandez-Pello, Temperature measurement of glowing embers with color pyrometry, Fire Technol. 55 (3) (2019) 1013–1026.
[28] B.Y. Lattimer, E. Bearinger, S. Wong, J.L. Hodges, Evaluation of models and important parameters for firebrand burning, Combust. Flame 235 (2022) 111619.
[29] S.L. Manzello, A. Maranghides, W.E. Mell, Firebrand generation from burning vegetation1, Int. J. Wildland Fire 16 (4) (2007) 458–462.
[30] D.K. Kim, P.B. Sunderland, Fire ember pyrometry using a color camera, Fire Saf. J. 106 (2019) 88–93.
[31] M. Tlemsani, Development and use of pixel-by-pixel pyrometry methods on smoldering wood embers and piles, University of Maryland, College Park, 2022.
[32] Y. Liu, J.L. Urban, C. Xu, C. Fernandez-Pello, Temperature and motion tracking of metal spark sprays, Fire Technol. 55 (2019) 2143–2169.
[33] F.P. Incropera, D.P. DeWitt, T.L. Bergman, A.S. Lavine, et al., Fundamentals of heat and mass transfer, vol. 6, Wiley New York, 1996.
[34] A. Warey, Influence of thermal contact on heat transfer from glowing firebrands, Case Stud. Therm. Eng. 12 (2018) 301–311.
[35] S.S. Wessies, J.C. Yang, Convective heat transfer correlation for a single surrogate firebrand and a simplified firebrand pile on a flat plate using naphthalene sublimation in heated air flow, Fire Saf. J 140 (2023) 103858.
[36] P. Cantor, M. Arruda, J. Firmo, F. Branco, Development of a standard firebrand accumulation temperature curve for residential wildfire protection system, RINENG 17 (2023) 100935.
[37] A.R. Bicelli, P. Cantor, M.R. Arruda, C. Tiago, E. Bernardes de Assis, F. Branco, Numerical assessment of standard firebrand accumulation curve when transferring temperature to contact surfaces, Appl. Sci. 13 (17) (2023) 9657.